Title
Nutrient Sensing in CD11c Cells Alters the Gut Microbiota to Regulate Food Intake and Body Mass.

Journal
Cell metabolism, 30(2)

ISSN
1550-4131

Authors
Chagwedera, D Nyasha
Ang, Qi Yan
Bisanz, Jordan E
et al.

Publication Date
2019-08-01

DOI
10.1016/j.cmet.2019.05.002

Peer reviewed

HHS Public Access
Author manuscript
Cell Metab. Author manuscript; available in PMC 2020 August 06.

Published in final edited form as:
Cell Metab. 2019 August 06; 30(2): 364–373.e7. doi:10.1016/j.cmet.2019.05.002.

Nutrient sensing in CD11c cells alters the gut microbiota to regulate food intake and body mass

D. Nyasha Chagwedera[1], **Qi Yan Ang**[2], **Jordan E. Bisanz**[2], **Yew Ann Leong**[1,3], **Kirthana Ganeshan**[1], **Jingwei Cai**[4], **Andrew D. Patterson**[4], **Peter J. Turnbaugh**[2,6], **Ajay Chawla**[1,5,6]

[1]Cardiovascular Research Institute, University of California, San Francisco, 94143-0795, USA

[2]Department of Microbiology & Immunology, University of California San Francisco (UCSF), San Francisco, CA 94143, USA.

[3]Centre for Inflammatory Diseases, Department of Medicine, School of Clinical Sciences at Monash Health, Monash University, Australia

[4]Center for Molecular Toxicology and Carcinogenesis, Department of Veterinary and Biomedical Sciences, The Pennsylvania State University, University Park, Pennsylvania, 16802, USA.

[5]Departments of Physiology and Medicine, University of California, San Francisco, 94143-0795, USA

[6]These authors contributed equally to this work

Summary

Microbial dysbiosis and inflammation are implicated in diet-induced obesity and insulin resistance. However, it is not known whether crosstalk between immunity and microbiota also regulates metabolic homeostasis in healthy animals. Here, we report that genetic deletion of tuberous sclerosis 1 (*Tsc1*) in CD11c^{+} myeloid cells (Tsc1$^{f/f}$CD11c^{Cre} mice), reduced food intake and body mass in the absence of metabolic disease. Cohousing and fecal transplant experiments revealed a dominant role for the healthy gut microbiota in regulation of body weight. 16S rRNA sequencing, selective culture, and reconstitution experiments further confirmed that selective deficiency of *Lactobacillus johnsonii* Q1–7 contributed to decreased food intake and body mass in Tsc1$^{f/f}$CD11c^{Cre} mice. Mechanistically, activation of mTORC1 signaling in CD11c cells regulated production of *L. johnsonii* Q1–7-specific IgA, allowing for its stable colonization in the gut. Together, our findings reveal an unexpected transkingdom immune-microbiota feedback loop for homeostatic regulation of food intake and body mass in mammals.

Lead Contact- Ajay Chawla: ajay.chawla@ucsf.edu.
AUTHOR CONTRIBUTION
D.N.C., Q.Y.A., J.E.B., Y.A.L, K.G., and J.C. designed and performed the main experiments. D.N.C., Q.Y.A., J.E.B., Y.A.L., K.G., J.C., A.D.T., P.J.T., and A C. conceived, discussed, interpreted the results, and wrote the paper.

DECLARATION OF INTERESTS
The authors declare no competing interests.

eTOC

Chagwedera et al. report that mTORC1 activation in CD11c cells reduces food intake and body weight in lean mice. The transfer of microbiota from control animals, in particular *L. johnsonii* Q1–7, rescues the phenotype suggesting the existence of transkingdom immune-microbiota circuits for homeostatic regulation of food intake and body mass in response to nutrient sensing in healthy mice.

Graphical Abstract

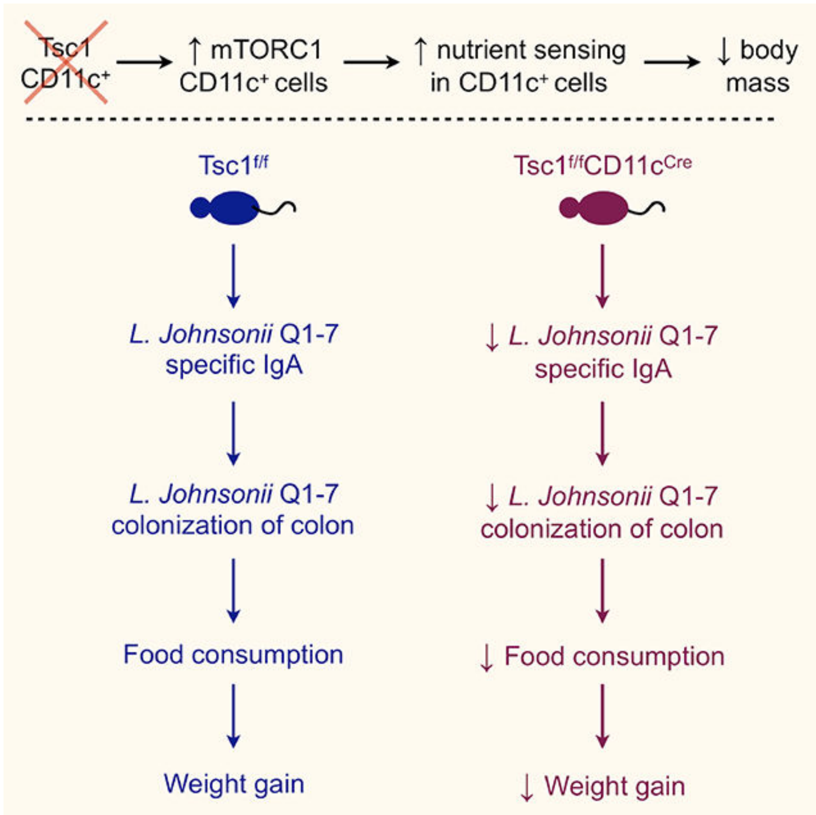

Introduction

Hypothalamic circuits regulate caloric intake, meal size, and energy expenditure to maintain body weight within a narrow range (Morton et al., 2014; Waterson and Horvath, 2015). This is principally mediated by the crosstalk between orexigenic and anorexigenic hypothalamic neurons expressing agouti-related protein (AGRP) and pro-opiomelanocortin (POMC), respectively. Since the activity of these neurons can be modulated by hormones (leptin, insulin, and glucagon-like peptide 1 (GLP1)), nutrients (glucose and fatty acids), and inflammatory cytokines (interleukin-6 and tumor necrosis factor-a), it provides a mechanism for regulating food intake and body weight under diverse set of dietary and environmental conditions.

In addition to these classical neuronal and hormonal pathways, previous studies in obese animals have implicated the immune system and the microbiota in regulation of body weight and insulin action (Heiss and Olofsson, 2018; Hotamisligil, 2017; Lee et al., 2018; Man et al., 2017; Maruvada et al., 2017; Schroeder and Backhed, 2016; Sonnenburg and Backhed, 2016). For example, obesity is associated with accumulation of $CD11c^{+}$ cells in white adipose tissue and microglial activation in the hypothalamus, which contribute to local and systemic inflammation, peripheral insulin resistance, and weight gain (Lumeng et al., 2007; Patsouris et al., 2008; Valdearcos et al., 2017). Moreover, in both mice and humans, diet-induced obesity alters the composition of the microbiota to increase energy harvest and systemic inflammation, factors which favor weight gain and insulin resistance, respectively (Ley et al., 2005; Nicholson et al., 2012; Turnbaugh et al., 2009; Turnbaugh et al., 2006). While these studies in obese animals demonstrate a pathogenic role for inflammation and microbial dysbiosis in metabolic diseases, the physiologic importance of these transkingdom interactions in healthy animals remains less well understood.

Here, we tested the hypothesis that nutrient sensing in innate immune cells regulates energy balance under physiologic conditions. We found that genetic activation of mechanistic target of rapamycin complex 1 (mTORC1) in CD11c cells, as in $Tsc1^{f/f}CD11c^{Cre}$ mice, alters the gut microbiota to reduce food intake and body weight in lean mice. Because these metabolic phenotypes were transmissible by the microbiota, in particular by *L. johnsonii* Q1–7, our findings suggest the existence of transkingdom immune-microbiota circuits for homeostatic regulation of food intake and body mass in healthy animals.

Results

Activation of mTORC1 signaling in CD11c cells reduces body mass and food intake

To investigate whether mTOR signaling in CD11c cells regulates glucose and energy homeostasis, we generated mice in which Tsc1, an inhibitor of the mTORC1 complex (Gonzalez and Hall, 2017; Saxton and Sabatini, 2017), was selectively deleted in CD11c cells (designated $Tsc1^{f/f}CD11c^{Cre}$ mice). Deletion of Tsc1 activated mTORC1 signaling in CD11c cells, as evidenced by increased phosphorylation of its downstream target S6 (Figure S1A–D). Although previous studies have implicated CD11c cells in pathogenesis of obesity-associated insulin resistance (Lumeng et al., 2007; Patsouris et al., 2008), nearly all of this work has been performed in animals housed under thermal stress conditions (ambient temperature (Ta) of 20–22°C). Since we and others have reported that thermal stress has a profound effect on systemic metabolism (Cannon and Nedergaard, 2011; Ganeshan and Chawla, 2017; Gordon, 2017; Tian et al., 2016), we performed all of our studies with mice housed at thermoneutrality (T_a = 30°C). We observed that, compared to their littermate controls ($Tsc1^{f/f}$ mice), thermoneutral male $Tsc1^{f/f}CD11c^{Cre}$ mice gained less weight on a high fat diet (Figure 1A), which was not associated with improvements in glucose tolerance or insulin sensitivity (Figure 1B, C). These results suggested that the primary metabolic effects stemming from mTORCl activation in CD11c cells were likely to be on body mass. To test this hypothesis, we repeated the studies with $Tsc1^{f/f}$ and $Tsc1^{f/f}CD11c^{Cre}$ mice that were fed a low-fat regular chow diet (24.5% protein, 13.1% fat, and 62.3% carbohydrates). We observed that male but not female $Tsc1^{f/f}CD11c^{Cre}$ mice had a lower body mass, which was independent of linear growth (Figure 1D and Figure S1E–H). Dual-energy X-ray absorptiometry (DEXA) revealed that reduction in both lean and fat mass contributed to the observed decrease in body mass in male $Tsc1^{f/f}CD11c^{Cre}$ mice (Figure 1E, F). Based on these observations, we chose to study the systemic effects of mTORC1 activation in CD11c cells using male mice that were fed a low-fat regular chow diet, which allowed us to avoid the pleiotropic effects of high fat diets on metabolic and immune systems, and the gut microbiota.

To identify the underlying mechanisms for the observed decrease in body mass, we quantified changes in energy expenditure in $Tsc1^{f/f}$ and $Tsc1^{f/f}CD11c^{Cre}$ male mice. We found that oxygen consumption and locomotor activity were similar in both groups of mice (Figure 1G, H and Figure S1I). Consistent with these observations, expression of thermogenic genes and thermogenic protein uncoupling protein 1 (UCP1) was not significantly different between the genotypes in brown adipose tissue (Figure S1J, K). We next asked whether deletion of Tsc1 in CD11c cells affected energy intake or absorption. Measurement of food intake revealed that food consumption was reduced by ~22% in $Tsc1^{f/f}CD11c^{Cre}$ mice (Figure 1I), whereas bomb calorimetry revealed that energy harvest was similar in both groups of mice (Figure 1J). This reduction in food intake was also observed during a fasting-refeeding paradigm (Figure 1K), which increased mTORC1 activity in hepatocytes but not CD11c cells in a microbiota-dependent manner (Figure 1K and S1L, M). Furthermore, comprehensive immunologic phenotyping of male $Tsc1^{f/f}CD11c^{Cre}$ mice demonstrated that changes in body mass were largely independent of systemic inflammation, hypothalamic microglial activation, and intestinal pathology, barrier dysfunction, and inflammation (Figure 1L, M, S1N, S2A–I, and S3A), there were some changes in the frequencies of innate and adaptive immune cells in lymphoid tissues (Table S1A). These findings collectively suggest that factors other than overt inflammation contribute to decreased food intake and smaller body mass in $Tsc1^{f/f}CD11c^{Cre}$ male mice.

The microbiota of $Tsc1^{f/f}CD11c^{Cre}$ mice reduces food intake and body mass

The gut microbiota is an important factor that regulates energy homeostasis. In mice, maternal transfer of the microbiota occurs at birth, which undergoes diversification and stabilization as animals wean from breast milk to solid food (Stappenbeck and Virgin, 2016). Because we observed that body mass of $Tsc1^{f/f}CD11c^{Cre}$ mice diverged from their littermate controls shortly after weaning (Figure 2A), we postulated that differences in the structure and function of gut microbial communities found in $Tsc1^{f/f}$ and $Tsc1^{f/f}CD11c^{Cre}$ mice might contribute to energy homeostasis. In support of this hypothesis, when $Tsc1^{f/f}$ and $Tsc1^{f/f}CD11c^{Cre}$ mice were cohoused instead of being separated at weaning, body mass, body composition, and food intake were not significantly different between the genotypes (Figure 2B–D). These differences in food intake and body mass between $Tsc1^{f/f}$ and $Tsc1^{f/f}CD11c^{Cre}$ mice could not be accounted for by variations in circulating levels of anorexigenic and orexigenic hormones, including leptin, GLP-1, and ghrelin (Figure S3B–F). These findings together suggested that the different microbial communities of $Tsc1^{f/f}$ and $Tsc1^{f/f}CD11c^{Cre}$ mice might contribute to body weight regulation.

Principal Coordinates Analysis (PCoA) of Bray Curtis dissimilarities generated from 16S rRNA sequence variants revealed that microbial communities were similar between Tsc1$^{f/f}$ and Tsc1$^{f/f}$CD11c^{Cre} mice at 3 weeks of age and became compositionally distinct as animals were housed separately for an additional 5 weeks (Figure 2E, F). However, these differences in microbial composition disappeared when the two genotypes were cohoused (Figure 2F), which coincided with the lack of difference in body mass between the genotypes (Figure 2B). Furthermore, analysis of sequence variants across three replicate experiments revealed four clades, including *Lactobacillaceae, Muribaculaceae*, *Lachnospiraceae* and *Ruminococcaceae*, that were differentially abundant in Tsc1$^{f/f}$CD11c^{Cre} mice compared to Tsc1$^{f/f}$ mice (Figure 2G). Because these shifts in microbial composition were independent of bacterial load and paralleled the changes in food intake (Figure S3G), it suggested a dominant role for the host microbiota in regulation of body mass. We tested this hypothesis by orally gavaging C57BL/6J mice with microbiota from Tsc1$^{f/f}$ or Tsc1$^{f/f}$CD11c^{Cre} mice. We observed that C57BL/6J mice receiving microbiota from Tsc1$^{f/f}$CD11c^{Cre} mice had lower food intake and body mass than those gavaged with microbiota from Tsc1$^{f/f}$ mice (Figure 2H, I). Together, these data suggest that Tsc1$^{f/f}$ and Tsc1$^{f/f}$CD11c^{Cre} mice harbor distinct microbial communities, whose adoptive transfer into C57BL/6J mice is sufficient to alter food intake and body mass.

Relative abundance of *Lactobacillus johnsonii* is reduced in microbiota of Tsc1$^{f/f}$CD11c^{Cre} mice

To narrow down the specific microbial taxa responsible for the regulation of the body mass in Tsc1$^{f/f}$CD11c^{Cre} mice, we performed two types of microbiota chase experiments. First, we asked whether transfer of Tsc1$^{f/f}$ mice to cages, which previously housed Tsc1$^{f/f}$CD11c^{Cre} mice, affected weight gain in Tsc1$^{f/f}$ mice (Figure 3A). We observed that the rate of change in body mass and food intake was not significantly different between Tsc1$^{f/f}$ mice transferred to new or Tsc1$^{f/f}$CD11c^{Cre} cages (Figure 3B, C). Second, we asked whether transfer of Tsc1$^{f/f}$CD11c^{Cre} mice to cages that previously housed Tsc1$^{f/f}$ mice might promote an increase in body mass (Figure 3D). Compared to control mice, we found that the rate of weight gain and food intake increased when Tsc1$^{f/f}$CD11c^{Cre} mice were transferred to cages that previously housed Tsc1$^{f/f}$ mice (Figure 3E, F). Similar changes in body mass and food consumption were observed when Tsc1$^{f/f}$CD11c^{Cre} mice were gavaged with donor microbiota from Tsc1$^{f/f}$ mice for 8 weeks (Figure 3G, H). Together, these data suggest that adoptive transfer of Tsc1$^{f/f}$ microbiota is sufficient to rescue weight gain in Tsc1$^{f/f}$CD11c^{Cre} mice, suggesting that chase or oral gavage might reconstitute microbes that are deficient in the microbiota of Tsc1$^{f/f}$CD11c^{Cre} mice.

To identify the microbes whose abundance regulates food intake and body mass in Tsc1$^{f/f}$CD11c^{Cre} mice, we used 16S rRNA gene sequencing to follow changes in gut microbial composition in Tsc1$^{f/f}$CD11c^{Cre} mice subjected to the microbiota chase experimental paradigm. We found that 3 sequence variants identified as *Lactobacillus, Rikenellaceae* RC9 group, and *Muribaculaceae* were significantly different between microbiotas of Tsc1$^{f/f}$CD11c^{Cre} mice that were transferred into new or Tsc1$^{f/f}$ cages (Figure 3D, 3I). However, *Lactobacillus* was the only clade that was reduced in microbiotas of Tsc1$^{f/f}$CD11c^{Cre} mice that were housed separately after weaning (Figure 3J, 2G). As multiple species could be mapped to these clades, we performed selective culture of *Lactobacillus* species followed by complete 16S rRNA gene sequencing of the isolated colonies. Based on the complete 16S rRNA gene sequence, the sequence variant of *Lactobacillus* that was cultured from stool of Tsc1 mice, referred here to as strain Q1–7, was identified as belonging to *L. johnsonii* with a 99% nucleotide identity match to the *L. johnsonii* type strain ATCC 33200. Furthermore, we found that the abundance of *L. johnsonii* group but not *Rikenellaceae* or *Muribaculaceae* increased over baseline in Tsc1$^{f/f}$CD11c^{Cre} mice during the course of the chase experiment and declined when the microbial chase with feces from Tsc1$^{f/f}$ mice was stopped (Figure 3K and Figure S3H, I). These findings suggest that abundance of *L. johnsonii* Q1–7 is causally linked to decreases in food intake and Tsc1$^{f/f}$CD11c^{Cre} mice might lack factors necessary for stable colonization by *L. johnsonii* Q1–7.

Reconstitution of *Lactobacillus* Q1–7 increases food intake and body mass in Tsc1$^{f/f}$CD11c^{Cre} mice

We next asked whether reconstitution of *L. johnsonii* Q1–7 into Tsc1^{ff}CD11c^{Cre} mice can increase food intake and body mass. Because oral gavage with *L. johnsonii* Q1–7 alone did not increase body weight in Tsc1$^{f/f}$CD11c^{Cre} mice (Figure S3J), we reasoned that colonization by *L. johnsonii* Q1–7 might be dependent on additional members of the gut microbiota for colonization. We tested this hypothesis by reconstituting mice with their microbial material plus *L. johnsonii* Q1–7. Indeed, we found that when Tsc1$^{f\ f}$CD11c^{Cre} mice were gavaged with fecal contents supplemented with *L. johnsonii* Q1–7 (5×10^9 cfu), body mass and food intake increased progressively over a period of 6 weeks (Figure 4A, B). Quantitative PCR verified increased relative abundance of *Lactobacillus* in microbiota of Tsc1$^{f/f}$CD11c^{Cre} mice (Figure S4A), indicating that oral introduction of *L. johnsonii* Q1–7 is sufficient to increase food intake and body mass in Tsc1$^{f/f}$CD11c^{Cre} mice. Since previous studies have suggested a role for microbiome-derived short chain fatty acids (butyrate, acetate, and propionate) and metabolites (succinate) in food intake and glucose homeostasis in obese animals (De Vadder et al., 2016; Frost et al., 2014; Koh et al., 2016; Schroeder and Backhed, 2016), we performed targeted metabolomics on cecal, fecal, and plasma samples from Tsc1$^{f/f}$ and Tsc1$^{f/f}$CD11c^{Cre} mice. Mass spectroscopy and NMR-based metabolomics revealed that levels of short chain fatty acids and other metabolites were largely similar in cecum, feces, and plasma of both groups of mice (Figure 4D and Figure S3K). These findings are consistent with our observations that energy extraction is similar in both genotypes (Figure 1J), suggesting that shifts in abundance of *L. johnsonii* Q1–7 likely regulate food intake by other mechanisms (Schroeder and Backhed, 2016).

To address the specificity of *L. johnsonii* Q1–7 in regulating food intake and body mass in Tsc1$^{f/f}$CD11c^{Cre} mice, we *de novo* genome sequenced this isolate and the related strain *Lactobacillus* strain I8–5. Based on phylogeny and whole genome average nucleotide identity, *L. johnsonii* Q1–7 and I8–5 were confirmed to belong to *L. johnsonii* and *L. reuteri* type, respectively (Figure S4B–D). To determine whether modulation of food intake and body mass was generalizable to the genus and/or species of *L. johnsonii*, we tested whether *L. johnsonii* ATCC 33200 or *L. reuteri* I8–5 could rescue food intake and body mass in Tsc1$^{f/f}$CD11c^{Cre} mice. We found that gavage of *L. reuteri* I8–5 or *L. johnsonii* ATCC 33200 for 6 weeks did not increase food intake or body mass of Tsc1$^{f/f}$CD11c^{Cre} mice (Figure 4D, E), indicating that the bioactivity of *L. johnsonii* Q1–7 is a strain specific trait. These observations led us to ask whether *L. johnsonii* Q1–7 harbored unique effector genes that might contribute to its effects on food intake. Comparison of annotated genes between the three *Lactobacillus* strains revealed that 126 candidates that were uniquely found in *L. johnsonii* Q1–7 (Figure 4F and Table S2). Amongst these candidate genes, choloylglycine hydrolase, lactococcin A, and glycotransferases Eps J and Eps F were particularly interesting because they are involved in bile acid metabolism, bacteriocin production, and extracellular polysaccharide, respectively (Table S2). While microbial metabolism of bile acids has been linked to regulation of body mass and energy expenditure in mice (Yao et al., 2018), bacteriocins and extracellular polysaccharides might influence food intake by altering the abundance of other bacterial species or via their interactions with host cells, respectively.

Finally, we sought to gain insights into the mechanisms through which changes in host immune function impact the abundance of *L. johnsonii* Q1–7. Secretory IgA directed against bacterial antigens has been proposed to shape intestinal microbial composition by multiple mechanisms, including inhibition of bacterial motility, reduction in bacterial fitness, exclusion of immune cells from the inner mucus layer, and creation of a specific mucosal niche to promote stable colonization by specific microbes (Cullender et al., 2013; Donaldson et al., 2018; Gutzeit et al., 2014; Peterson et al., 2007). Because antigen capture and presentation by lamina propria macrophages and dendritic cells contributes to the development of IgA secreting plasma cells (Cerovic et al., 2014; Ko and Chang, 2015), we hypothesized that deletion of Tsc1 in CD11c cells might alter the amount or specificity of secreted IgA against *L. johnsonii* Q1–7. We found that while the concentration of free IgA in stool was similar between Tsc1$^{f/f}$ and Tsc1$^{f/f}$CD11c^{Cre} mice (Figure 4G), IgA directed against *L. johnsonii* Q1–7 was reduced in Tsc1$^{f/f}$CD11c^{Cre} mice. For example, in both separated and cohoused animals, we found that the stool of Tsc1$^{f/f}$CD11c^{Cre} mice contained less IgA that specifically bound *L. johnsonii* Q1–7 (Figure 4H, I). This seemed to be specific for *L. johnsonii* Q1–7 because binding to an unrelated bacterial strain *Bifidobacterium pseudolongum* B4, a bacterial strain isolated from the original experimental fecal material whose abundance was similar in both groups of mice, was unaffected (Figure 4J). Together, these data suggest that reduced production of IgA directed against *L. johnsonii* Q1–7 might prevent it from stably colonizing the gastrointestinal tract of Tsc1$^{f/f}$CD11c^{Cre} mice, as was observed during the microbiota chase experiment (Figure 3K).

CD11c is highly expressed in lamina propria macrophages and dendritic cells, which are critical for maintaining intestinal and commensal homeostasis (Cerovic et al., 2014). To gain insights into how activation of mTORC1 signaling in CD11c cells might regulate mucosal secretion of IgA by B cells, we began by characterizing the innate and adaptive immune populations in the lamina propria of small intestines and colon, Peyer's patches, and mLNs. We found that deletion of *Tsc1* in CD11c cells did not significantly affect lamina propria dendritic cell subsets (Table S1B), but preferentially affected resident intestinal macrophages of the small bowel and colon. For example, in the proximal small intestines, we observed reduction in tissue resident macrophages (CD11c^{+}MHCn^{+}CD64^{+}Ly6C^{-}CD11b^{+}) accompanied by an increase in precursor monocytic cells (CD11c^{+}MHCn^{+}CD64^{+}Ly6C^{+}CD11b^{-}), suggestive of a potential block in maturation of lamina propria macrophages

(Figure S4E, F). A similar defect in maturation of tissue resident macrophages was observed in the colon but not the Peyer's patches and mLNs (Figure 4K and Table S1A). Because intestinal macrophages can sample luminal contents to modulate adaptive immunity, we quantified T- and B-cells in the lamina propria of the colon. We found that the frequency of Tregs ($FOXP3^{+}$), Th1 (T-bet^{+}), and Th17 ($ROR\gamma t^{+}$) cells was not significantly different between the genotypes, whereas total and IgA^{+} B cells were increased in the colon (Figure S4G, 4L, and Table S1B). Taken together, these results suggest that activation of mTORC1 signaling in CD11c cells alters IgA secretion at mucosal sites, resulting in shifts in microbial communities to decrease food intake and body mass (Figure 4M).

Discussion

Previous studies have highlighted a role for inflammation and microbial dysbiosis in metabolic dysfunction associated with disease states of obesity and insulin resistance (Hotamisligil, 2017; Lee et al., 2018; Maruvada et al., 2017; Schroeder and Backhed, 2016; Sonnenburg and Backhed, 2016). However, the physiologic importance of these systems in maintenance of energy balance in healthy animals is less well understood. The data presented here provide an example of a transkingdom circuit involving CD11c cells and the gut bacterium *L. johnsonii* Q1–7, which regulates food intake and body weight in lean animals (Figure 4M). Utilization of a modified set of Koch's postulates allowed us to identify this transkingdom circuit in $Tsc1^{f/f}CD11c^{Cre}$ mice. First, we found that the reduced food intake and body mass in $Tsc1^{f/f}CD11c^{Cre}$ mice was dependent on the host microbiota. Second, 16S rRNA gene sequencing of cohoused and microbiota chased mice led to the identification of *L. johnsonii* as being selectively depleted in microbiota of $Tsc1^{f/f}CD11c^{Cre}$ mice. Third, *L. johnsonii* Q1–7 was selectively cultured from the microbiota of $Tsc1^{f/f}$ mice, and its reconstitution into $Tsc1^{f/f}CD11c^{Cre}$ mice increased food intake and body mass. Fourth, supplementation with *L. reuteri* I8–5, a *Lactobacillus* strain whose abundance was not significantly different between the genotypes, or *L. johnsonii* ATCC 33200 failed to restore food intake and body mass in $Tsc1^{f/f}CD11c^{Cre}$ mice. And fifth, $Tsc1^{f/f}CD11c^{Cre}$ mice produced lower levels of *L. johnsonii* Q1–7-specific IgA, which is likely necessary for the stable colonization by *L. johnsonii* Q1–7 in its microbial niche.

A major challenge in the microbiome field is to identify specific microbial pathways and products that modulate host physiology and contribute to pathogenesis of disease (Maruvada et al., 2017; Sonnenburg and Backhed, 2016). Although previous studies have implicated microbiome-derived short chain fatty acids, such as acetate, butyrate, and propionate, in regulation of food intake and weight gain (Frost et al., 2014; Koh et al., 2016), the levels of these and other metabolites were not significantly different between $Tsc1^{f/f}$ and $Tsc1^{f/f}CD11c^{Cre}$ mice (Figure 4C and S3J). In line with these observations, circulating levels of hormones that regulate satiety and meal size, such as leptin, GLP-1, and ghrelin failed to account for the effects *L. johnsonii* Q1–7 on feeding behavior (Figure S3A–E). Together, these findings suggest that immune-microbiome interactions might employ distinct mechanisms to maintain metabolic homeostasis in healthy animals.

Comparative genomics between the bioactive *L. johnsonii* Q1–7 and the two inactive strains *L. reuteri* I8–5 and *L. johnsonii* ATCC 33200 provides potential insights into how *L.*

johnsonii Q1–7 might regulate food intake and body mass in mice. For example, comparison of these three *Lactobacillus* genomes identified 126 candidate effectors that were specifically found in *L. johnsonii* Q1–7 (Figure 4F and Table S2). Amongst these candidates, genes encoding proteins involved in the metabolism of bile acids, bacteriocin production, and extracellular polysaccharide biosynthesis are particularly interesting. While modification of primary bile acids into secondary bile acids by the gut microbiome provides a direct means of regulating metabolic homeostasis (Tremaroli and Backhed, 2012; Yao et al., 2018), bacteriocin and extracellular polysaccharides may have indirect effects on the host by shaping the gut microbiota or host immune responses, respectively. The functional importance of these candidates will require generation of many new *Lactobacillus* strains that lack these genetic effectors and testing them individually in reconstitution experiments with $Tsc1^{f/f}CD11c^{Cre}$ mice, an area that is worthy of future investigations.

Finally, the results presented here highlight how the microbiome interacts with the host genotype to regulate its phenotypes. For example, many of the immunologic changes observed in the spleen, Peyer's patches, and mLNs of separately housed $Tsc1^{f/f}CD11c^{Cre}$ mice were reversed when $Tsc1^{f/f}CD11c^{Cre}$ mice were cohoused with their control littermates (Table S1A). These findings not only highlight a crucial role for gene (*Tsc1* in CD11c cells)-environment (microbiome) interactions in shaping the host immune responses, but also provide a potential explanation for how the same genotype can give rise to divergent phenotypes (Luo et al., 2017; Wang et al., 2013).

Limitations of Study

There are some limitations of the present study. First, it is well appreciated that the host-microbiome interactions are dynamic and dependent on the host environment. Thus, it remains unknown how environmental stimuli (diet, ambient temperature, and housing facility) might impact the microbial composition and metabolic phenotypes of $Tsc1^{f/f}CD11c^{Cre}$ mice. Second, CD11c is broadly expressed on dendritic cells and a subset of macrophages, which reside at barrier surfaces and in lymphoid tissues. Thus, the precise location and mechanisms by which CD11c cells regulate abundance of *L. johnsonii* Q1–7 in the gut remain to be elucidated. Third, while our findings suggest that activation of mTORC1 signaling in CD11c cells alters B cell responses, deeper understanding of how strain specific IgA responses, including specificity, affinity, and titer, are regulated will require identification of specific antigens on *L. johnsonii* Q1–7, and their cognate T- and B-cell receptors. And fourth, it remains to be determined whether the transkingdom circuit identified here is representative of a broader mechanism for homeostatic regulation of food intake and body mass in mammals.

STAR Methods

CONTACT FOR REAGENT AND RESOURCE SHARING

Further information and requests for resources and reagents should be directed to and will be fulfilled by the Lead Contact, Ajay Chawla (ajay.chawla@ucsf.edu).

EXPERIMENTAL MODEL AND SUBJECT DETAILS

Mice—All animal studies were conducted under an approved Institutional Animal Care and Use Committee (IACUC) protocol at University of California, San Francisco (UCSF). Mice were housed at 30°C after weaning (unless otherwise indicated) in Darwin or Power Scientific environmental chambers under a 12-hr light:dark cycle. $Tsc1^{f/f}$ and $CD11c^{Cre}$ mice were purchased from Jackson Laboratories, backcrossed onto C57BL/6J background (*Nnt* null) for 10 generations, and used to generate $Tsc1^{f/f}$ $CD11c^{Cre}$ mice. Littermate $Tsc1^{f/f}$ and $Tsc1^{f/f}CD11c^{Cre}$ mice were either separated at weaning or continually cohoused for the duration of the experiments. Mice were fed normal chow diet (5053, Pico labs) or high fat diet (D12492i, Research Diets). For microbiota chase experiments, mice were moved to a new cage or a cage that previously housed mice every day for duration of the experiment. Male mice (2–20 weeks of age) were used in the experiments reported here because we did not observe differences in body mass in female mice.

METHOD DETAILS

Food intake—Successive food consumption was calculated using the formula: [(Food mass) on Day(N) - (Food mass) on Day(N+1)], and values were normalized for the number of mice per cage. The same number of mice per cage were compared between experimental groups to minimize the impact of housing density on food consumption.

Energy expenditure and body composition analysis—Body composition (fat and lean mass) analysis were performed on anesthetized mice using Dualenergy X-ray absorptiometry (DEXA). For measurement of energy expenditure, food intake, and locomotor activity, mice were placed in CLAMS (Columbus Instruments) cages that housed in an environmental chamber set at 30°C. After acclimatization for one day, data on oxygen consumption, locomotor activity, and food intake was collected every 22 minutes.

Glucose and insulin tolerance tests—For glucose and insulin tolerance tests, mice were intraperitoneally injected with glucose (1.5g/kg of body weight) after 14h fast or insulin (1U/kg of body weight) after 6h fast, and blood glucose was measured at regular intervals using tail blood.

Bomb calorimetry—Fecal samples were collected and lyophilized to obtain dried mass. Approximately, 200 mg of dried stool was pressed into a pellet using a pellet press. Gross energy content was measured using a semimicro oxygen bomb in an isoperibol calorimeter. The calorimeter energy equivalent factor was determined using benzoic acid standards. Data are presented as a percentage of energy consumed by each genotype.

Quantitative RT-PCR—CD11c cells were purified from lamina propria (LP) of small intestine (SI) and colon using MACs (Miltenyi) separation following manufacturer's instructions. As per manufacturer's protocols, fecal DNA or tissue RNA was extracted using Bioline Fecal DNA or RNA kits, respectively. RNA was reverse transcribed into cDNA using qScript cDNA Supermix (Quanta), and quantitative PCR was performed on CFX384 real-time PCR detection system (Bio-rad). Relative expression levels were determined using the AACt method with 36B4 or GAPDH serving as an internal reference. *Lactobacillus* enumeration was normalized to stool weight. Primers used are listed in Supplemental Table 3.

Histology—Brown fat, small intestines, and colons were fixed in 10% formalin for 4–24 hours and stored at 4°C in 20% sucrose in PBS. Paraffin embedded tissues were sectioned at 5 µm, stained with hematoxylin and eosin, and imaged using an Olympus BX41 equipped with a Digital Sight DS-Fi1 camera (Nikon).

Immunoblotting—Snap-frozen tissues were homogenized in modified RIPA buffer (420 mM NaCl, 1% NP-40, 0.1% SDS, 0.5% sodium deoxycholate, 50 mM Tris pH 7.5, and protease inhibitor cocktail) using a TissueLyser II (Qiagen). Total protein was separated by SDS-PAGE, transferred to nitrocellulose membranes, and probed with primary anti-UCPl and secondary anti-IgG HRP antibodies. Immunoblotted proteins were detected using SuperSignal West Pico Chemiluminescent Substrate (Thermo Scientific).

Culture of bone marrow dendritic cells (BMDCs)—Bone marrow cells were flushed from femurs and tibias of $Tsc1^{f/f}$ and $Tsc1^{f/f}CD11c^{Cre}$ mice, and cultured in RPMI 1640 supplemented with 10% FBS, 10 mM HEPES pH 7.0, 100 U/ml penicillin, 1000 U/ml streptomycin, 20 mM l-glutamine, and 20 ng/ml GM-CSF. On day 3 of culture, half the medium was replaced with fresh medium. On day 7, BMDCs were used for experiments or flow cytometric analysis.

Flow cytometry and plasma cytokines—Spleens, Peyer's patches, and mesenteric lymph nodes were smashed through a 70µm strainer in FACS buffer and stained with antibodies listed in the Resource Table. Liver was digested using liver digest buffer (HBSS +CaCl2, 1% Dispase, 0.5% Collagenase II) at 37°C. Hepatocytes were pelleted by differential centrifugation at 50g for 5 minutes. For intracellular staining, cells were permeabilized in ice cold 100% methanol at RT for 1 hour and then stored at −80C overnight. Permeabilized cells were washed 3 times in FACS buffer and stained for pS6. Small intestine and colon flow cytometric analyses were performed as described previously (Belinson et al., 2016). Briefly, proximal and distal intestine and colon were dissected. Colon length was measured and numbers of Peyer's patches (PPs) and intestinal lymphoid structures (ILSs) were removed and counted. The gut tissue was then shaken in three times in 20 ml cold PBS, washed twice for 20 minutes at 37°C in 20 ml of Ca^{2+}/Mg^{2+}efree HBSS containing 5 mM DTT, 5 mM EDTA, 10 mM HEPES, and 2% FCS, followed by washing in 20 ml of Ca^{2+}/Mg^{2+}-replete HBSS containing 10 mM HEPES with 2% FCS. Tissues were then digested for 30 minutes at 37°C in 5 ml of Ca^{2+}/Mg^{2+}-replete HBSS containing 10 mM HEPES, 2% FCS, 30 µg/ml DNase, 0.1 Wünsch/ml LibTM (Roche), homogenized in C tubes using a gentleMACS tissue dissociator (Miltenyi), and then passed through a 100-µm filter. The filtrate was separated in a 40%/90% Percoll gradient and stained for innate and adaptive immune cells. Antibody sources and concentrations used are listed in the Resources Table. Data was acquired using FACSVerse (Becton Dickinson) and analyzed using FlowJo software. Plasma cytokine levels were measured by cytometric bead array-mouse inflammation kit (BD Biosciences, San Jose, CA) or IFNα kit (Ebiosciences) as per manufacturer's instructions.

Intestinal macromolecular permeability assay—Intestinal macromolecular permeability assay was performed in mice after a 5h fast. Mice were orally gavaged with 40μg of fluorescein isothiocyanate (FITC)-dextran (4kDA/g body weight), and 5 hours later, FITC-dextran was detected in plasma samples using flow cytometry.

Measurement of GLP-1, leptin, and ghrelin—For measurement of active GLP-1, mice were fasted for 6 hours and given 2g/kg glucose by oral gavage. 15 mins later, mice were bled retro-orbitally using ice-cooled heparinized capillary tubes. DPP4 inhibitor was immediately added at 10μL per ml of blood. Samples were centrifuged at 1,000g for 10 mins and GLP-1 levels measured according to manufacturer's protocol. For measurement of leptin and active ghrelin, mice were bled retro-orbitally at 7am, blood was centrifuged at 8,000g for 8 mins. Resulting plasma was diluted 5× with PBS and leptin levels measured according to manufacturer's instructions.

Short chain fatty acids quantitation by GC-MS—Short chain fatty acids were quantified with a previously described propyl esterification method using Agilent 7890A gas chromatograph coupled with Agilent 5975 mass spectrometer (Agilent Technologies Santa Clara, CA). Briefly, 50 mg cecal/fecal samples or 300 μL of serum collected were mixed with 1 mL of 5 mM NaOH containing 10 μg/mL internal standard hexanoic acid-6,6,6-d3 (C/D/N Isotopes Inc, Pointe-Claire, Quebec, Canada), homogenized (Bertin Technologies, Rockville, MD) at 6500 rpm for 1 minute until thoroughly homogenized. 1.0 mm diameter Zirconia/Silica beads (BioSpec, Bartlesville, OK) were added for through homogenization (Zheng et al., 2013). The homogenized samples then were centrifuged (Eppendorf, Hamburg, Germany) at 13,200 × g, 4 °C, 20 minutes. The supernatant was taken and mixed with an aliquot of 500 μL of 1-propanol/pyridine (v/v=3:2) solvent. 100 μL of derivatization reagent propyl chloroformate was added slowly following a brief vortex for 1 minute. Samples were derivatized in an incubator (Thermo Scientific, Marietta OH) at 60 °C for an hour. The derivatized samples were extracted with a two-step hexane extraction (300 μL + 200 μL). A total 500 μL of upper layer was transferred to a glass auto sampler vials for GC-MS analysis. A calibration curve with pure standards was drafted for quantitation as described (Cai et al., 2016).

^{1}H NMR-based global metabolomics—Cecal content, feces and serum metabolites were extracted as previously described (Cai et al., 2016; Shi et al., 2013). ^{1}H NMR spectra were recorded at 298 K on a Bruker Avance III 600 MHz spectrometer equipped with an inverse cryogenic probe (Bruker Biospin, Germany). NMR spectra of cecal and fecal samples were acquired using the first increment of NOESY pulse sequence with presaturation (Bruker 1D noesygppr1d pulse sequence). The serum spectra were acquired with a Carr-Purcell-Meiboom-Gill pulse sequence [recycle delay-90°-(τ−180°-τ)$_n$-acquisition]. Quality of all spectra were improved by phase adjustment, baseline correction and calibration using Topspin 3.0 (Bruker Biospin, Germany). The spectral region δ 0.50–9.50 was integrated into bins with equal width of 0.004 ppm (2.4 HZ) using AMIX package (V3.8, Bruker Biospin) for relative concentration analysis. The metabolites were assigned based on published results (Cai et al., 2016; Dong et al., 2013; Tian et al., 2012).

IgA Binding Assay—IgA was isolated by homogenizing stool in PBS containing protease inhibitor (0.1 mg/μl) followed by centrifugation at 400g. Supernatant was collected by filtration through a 70 μm strainer followed by centrifugation at 8000g to pellet the bacteria. IgA concentration in the supernatant was quantified by Mouse IgA ELISA (Bethyl Laboratories). For quantifying IgA bound bacteria, bacterial pellets were resuspended in PBS supplemented with 5% goat serum and SYTO BC (ThermoFisher Technologies) followed by incubation for 15 minutes on ice. Anti-IgA-Alexa Fluor 647 (Southern Biotech) was added for 20 minutes on ice. Samples were washed and resuspended in PBS with DAPI (ThermoFisher Technologies) for flow cytometric analysis. Data was acquired on FACSVerse (Becton Dickinson) using a low FSC and SSC threshold (in log scale) to allow for bacterial detection and analyzed using FlowJo software. Samples were gated as FSC^{+}SSC^{+}SYTOBC^{+}DAPI^{-} and assessed for IgA staining. IgA-*L. johnsonii* Q1–7 or *B. pseudolongum* B4 binding assay was performed as previously described (Moor et al., 2016). Briefly, 25μl of 5×10^{6}cfu/ml *L. johnsonii* Q1–7 or *B. pseudolongum* B4 was incubated with 25μl of free IgA (3μg/ml), which was obtained from stool of Tsc1$^{f/f}$ and Tsc1$^{f/f}$CD11c^{Cre} mice, in a V-bottom-96 well plate overnight at 4°C. The incubated samples were washed in bacterial flow cytometry buffer (PBS with 2% BSA (wt/vol) and 0.02% sodium azide (wt/vol) by centrifugation at 4,000g for 10min at 4°C. The samples were then stained with 50μl of 10μg/ml IgA-FITC antibody (BD Biosciences) at RT for 15min, washed, and bacterial pellets were resuspended in 300μl bacterial flow cytometry buffer. Data was acquired using FACSVerse (Becton Dickinson) with a low FSC and SSC threshold to allow bacterial detection and analyzed using FlowJo software. FSC and SSC were set to log scale and gated bacteria were assessed for IgA binding.

Quantification of Bacterial Load—DNA templates were diluted 10-fold before quantitative PCR (qPCR) of 16S rRNA gene copies was performed. qPCR was carried out in triplicate 10uL reactions with 200nM 891F/1003R primers and 5’-Cy5 fluorogenic probe, performed on CFX384 real-time thermocycler (Bio-rad) with iTaq Universal Probes Supermix (Bio-rad) according to the manufacturer’s instructions and an annealing temperature of 60°C. Mean Ct values of triplicate reactions were taken for relative quantification of 16S rRNA gene copies in fecal DNA between genotype.

16S rRNA Gene Sequencing—Mouse fecal pellets were homogenized with bead beating for 5 min (Mini-Beadbeater-96, BioSpec) using beads of mixed size and material (Lysing Matrix E 2mL Tube, MP Biomedicals) in the digestion solution and lysis buffer of a Wizard SV 96 Genome DNA kit (Promega). The samples were then centrifuged for 10 min at 16,000g and the supernatant was transferred to the binding plate. The DNA was then purified according to the manufacturer’s instructions. 16S rRNA gene PCR was carried out using GoLay-barcoded 515F/806R primers (Caporaso et al., 2012). 2μL of DNA was combined with 25 μL of AmpliTaq Gold 360 Master Mix (Fisher Scientific), 5 μL of primers (2μM each GoLay-barcoded 515/806R), and 18μL H_2O. Amplification was as follows: 10 min 95°C, 30× (30s 95°C, 30s 50°C, 30s 72°C), and 7 min 72°C. Amplicons were quantified with PicoGreen (Quant-It dsDNA; Life Technologies) and pooled at equimolar concentrations. Aliquots of the pools were then column (MinElute PCR Purification Kit; Qiagen) and gel purified (QIAquick Gel Extraction Kit; Qiagen). Libraries were then quantified (KAPA Library Quantifcation Kit; Illumina) and sequenced with a 600 cycle MiSeq Reagent Kit (251×151; Illumina) with 20–50% PhiX.

Isolation and identification of bacterial species—*Lactobacillus* species were isolated from stool of Tsc1$^{f/f}$ mice by plating diluted stool on MRS agar with and without vancomycin (50μg/mL) followed by incubation at 37°C for 24 hours under anaerobic conditions using BBL GasPak 100 EZ gas generating container (Becton Dickinson). 11 colonies were randomly selected for 16S rRNA sequencing. The Q1–7 and I8–5 isolates were putatively identified as *L. johnsonii* and *L reuteri* by Sanger sequencing the 8F-1543R amplicon of 16S rRNA gene and 100% identities to amplicon sequence variants of interest. *Lactobacillus* isolates were stored in MRS media with 20% glycerol at −80°C. For oral gavage, *Lactobacillus* strains Q1–7, I8–5, and ATCC 33200 were grown in MRS broth and concentrated by centrifugation at 8,000g for 5min. Mice were orally gavaged with 5×10^9 cfu of *Lactobacillus* strains Q1–7, I8–5, or ATCC 33200 resuspended in 100 μL of saline six days a week. *Bifidobacterium* species were isolated from stool by plating diluted stool on TOS-propionate agar (Sigma Aldrich 43314) containing mupirocin (50mg/mL, Sigma Aldrich 69732) followed by incubation at 37°C for 24 hours under anaerobic conditions using BBL GasPak 100 EZ gas generating container (Becton Dickinson). Single colonies were grown in brain heart infusion (BHI) broth under anaerobic conditions and the identity of the isolated bacteria was confirmed by Sanger sequencing of the 16S rRNA gene before use in *in vitro* experiments.

Fecal microbiota transplantation—Antibiotics (vancomycin hydrocholoride (5 mg/ml), metronidazole (10 mg/ml), ampicillin (10mg/ml), and neomycin trisulfate salt hydrate (10 mg/ml)) were administered to mice in drinking water for 24 hours. Fresh feces were collected from three to four mice in PBS (supplemented with 0.05% cysteine, 1μg/ml vitamin K, 15% glycerol, 5 μg/ml hemin), gently homogenized, pooled, and passed through a 100-μm cell strainer. The suspension was administered by oral gavage six days a week in mice treated with antibiotics.

QUANTIFICATION AND STATISTICAL ANALYSIS

Statistical analysis—Data were analyzed using Prism (GraphPad) and are presented as mean±SEM. Statistical significance was determined using the unpaired two-tailed Student's *t* test for single variables and two-way ANOVA for two variables. A *p*-value of <0.05 was considered to be statistically significant. No methods were used to determine if data met assumptions of statistical approach. Statistical parameters described above can be found in the figures.

16S rRNA Gene Analysis—Raw data was deposited in the NCBI Sequence read archive under SRP154475. Reads were demultiplexed using QIIME v1.9.1 (split_libraries_fastq.py) before denoising and processing with DADA2 v1.1.5 under MRO v3.2.5 (Callahan et al., 2016). Taxonomy was assigned using the DADA2 implementation of the RDP classifier using the DADA2 formatted training sets for SILVA123 (benjjneb.github.io/dada2/assign.html) (Wang et al., 2007). A phylogenetic tree was constructed using MUSCLE v3.8.31 using the FastTree algorithm with midpoint rooting. Sequence variants were filtered such that they were present in more than one sample with at least a total of 10 reads. Diversity metrics were generated using Vegan v2.5–2 with principal coordinate analysis (PCoA) carried out with Ape v5.1. The Wald test in DESeq2 package (v1.20) was used to analyze differential abundances on count data. PhILR transformation was carried out with the package philr v1.6 as described and analyzed using *t test* with multiple testing correction across features/nodes tested (Silverman et al., 2017). For the separated housing experiments, significant nodes and sequence variants were visualized on a phylogenetic tree using the ggtree package v1.12. For the microbiota chase experiment, variance stabilizing transformation (DESeq2 package v1.20) was applied on count data, and time-course analysis was carried out using linear mixed effect models (lmerTest v3.0–1) with mouse as a random effect to account for repeated sampling across time using the with a 0.05 Benjamini-Hochberg false discovery rate cutoff for significance.

Comparative genomics and phylogenetic analysis—The genomes *of L. reuteri* I8–5 and *L. johnsonii* Q1–7 were *de novo* sequenced and assembled and are available via NCBI bioproject PRJNA482000. Genomic DNA was extracted from broth cultures (MRS, 37°C anaerobic for 24h) and libraries were prepared using the Illumina Nextera XT kit and sequenced on both an Illumina MiSeq and NovaSeq run with 2×300 and 2×140 chemistry (Koppel et al., 2018). Resulting reads were filtered and trimmed of adapters before removal of PhiX contamination (Chen et al., 2018; Langmead and Salzberg, 2012). Finally overlapping reads were identified and merged using vsearch version 2.4.4 (10.7717/peerj.2584). Reads were assembled using SPAdes 3.13.0 (Bankevich et al., 2012), and annotated using the PROKKA pipeline (Seemann, 2014). Overlapping gene content was identified using gene ortholog finding tool Proteinortho5 with a minimum identity of 25%, coverage of 50%, and e-value of 1e-5 (Lechner et al., 2011). The phylogenetic tree was created using PhyloPhlAn using a set of publicly available assemblies identified through the Pathosystems Resource Integration Center (PATRIC) catalogue (www.patricbrc.org) using *Enterococcus faecalis* ATCC 19433 (GCA_000392875.1) as an outgroup (Segata et al., 2013).

DATA AND SOFTWARE AVAILABILITY

The 16s rRNA amplicon sequencing, and genomic sequences of *Lactobacillus johnsonii Q1–7* and *Lactobacillus reuteri I8–5* have been deposited at the Sequence Reach Archive under the accession number: PRJNA482000.

Supplementary Material

Refer to Web version on PubMed Central for supplementary material.

Acknowledgments

We thank members of the Chawla laboratory and A. Loh for comments on the manuscript, A. Savage for assistance with SI and colon flow cytometry, and X. Cui for assistance with mouse husbandry. The authors' work was supported by grants from NIH (DK094641 and DK101064 to A.C.; C2273232 and HL122593 to P.J.T.). Stipend support was provided by NIH NIDDK and UCSF MSTP (F31DK112669 and T32GM007618) to D.N.C. Y.A.L. was supported by NHMRC (GNT1142229), K.G. by Hillblom Fellowship and CVRI T32 grant, Q.Y.A by Agency for Science, Technology and Research, Singapore (National Science Scholarship), and J.E.B. by postdoctoral fellowship from National Science and Engineering Research Council of Canada. The authors declare that they have no competing financial interests.

References

Bankevich A, Nurk S, Antipov D, Gurevich AA, Dvorkin M, Kulikov AS, Lesin VM, Nikolenko SI, Pham S, Prjibelski AD, et al. (2012). SPAdes: a new genome assembly algorithm and its applications to single-cell sequencing. J Comput Biol 19, 455–477. [PubMed: 22506599]

Belinson H, Savage AK, Fadrosh D, Kuo YM, Lin D, Valladares R, Nusse Y, Wynshaw-Boris A, Lynch SV, Locksley RM, et al. (2016). Dual epithelial and immune cell function of Dvl1 regulates gut microbiota composition and intestinal homeostasis. JCI Insight 1.

Cai J, Zhang L, Jones RA, Correll JB, Hatzakis E, Smith PB, Gonzalez FJ, and Patterson AD (2016). Antioxidant Drug Tempol Promotes Functional Metabolic Changes in the Gut Microbiota. J Proteome Res 15, 563–571. [PubMed: 26696396]

Callahan BJ, McMurdie PJ, Rosen MJ, Han AW, Johnson AJ, and Holmes SP (2016). DADA2: High-resolution sample inference from Illumina amplicon data. Nature methods 13, 581–583. [PubMed: 27214047]

Cannon B, and Nedergaard J (2011). Nonshivering thermogenesis and its adequate measurement in metabolic studies. The Journal of experimental biology 214, 242–253. [PubMed: 21177944]

Caporaso JG, Lauber CL, Walters WA, Berg-Lyons D, Huntley J, Fierer N, Owens SM, Betley J, Fraser L, Bauer M, et al. (2012). Ultra-high-throughput microbial community analysis on the Illumina HiSeq and MiSeq platforms. ISME J 6, 1621–1624. [PubMed: 22402401]

Cerovic V, Bain CC, Mowat AM, and Milling SW (2014). Intestinal macrophages and dendritic cells: what's the difference? Trends Immunol 35, 270–277. [PubMed: 24794393]

Chen S, Zhou Y, Chen Y, and Gu J (2018). fastp: an ultra-fast all-in-one FASTQ preprocessor. Bioinformatics 34, i884–i890. [PubMed: 30423086]

Cullender TC, Chassaing B, Janzon A, Kumar K, Muller CE, Werner JJ, Angenent LT, Bell ME, Hay AG, Peterson DA, et al. (2013). Innate and adaptive immunity interact to quench microbiome flagellar motility in the gut. Cell Host Microbe 14, 571–581. [PubMed: 24237702]

De Vadder F, Kovatcheva-Datchary P, Zitoun C, Duchampt A, Backhed F, and Mithieux G (2016). Microbiota-Produced Succinate Improves Glucose Homeostasis via Intestinal Gluconeogenesis. Cell Metab 24, 151–157. [PubMed: 27411015]

Donaldson GP, Ladinsky MS, Yu KB, Sanders JG, Yoo BB, Chou WC, Conner ME, Earl AM, Knight R, Bjorkman PJ, et al. (2018). Gut microbiota utilize immunoglobulin A for mucosal colonization. Science 360, 795–800. [PubMed: 29724905]

Dong FC, Zhang LL, Hao FH, Tang HR, and Wang YL (2013). Systemic Responses of Mice to Dextran Sulfate Sodium-Induced Acute Ulcerative Colitis Using H-1 NMR Spectroscopy. Journal of Proteome Research 12, 2958–2966. [PubMed: 23651354]

Frost G, Sleeth ML, Sahuri-Arisoylu M, Lizarbe B, Cerdan S, Brody L, Anastasovska J, Ghourab S, Hankir M, Zhang S, et al. (2014). The short-chain fatty acid acetate reduces appetite via a central homeostatic mechanism. Nature communications 5, 3611.

Ganeshan K, and Chawla A (2017). Warming the mouse to model human diseases. Nature reviews. Endocrinology 13, 458–465.

Gonzalez A, and Hall MN (2017). Nutrient sensing and TOR signaling in yeast and mammals. The EMBO journal 36, 397–408. [PubMed: 28096180]

Gordon CJ (2017). The mouse thermoregulatory system: Its impact on translating biomedical data to humans. Physiol Behav 179, 55–66. [PubMed: 28533176]

Gutzeit C, Magri G, and Cerutti A (2014). Intestinal IgA production and its role in host- microbe interaction. Immunological reviews 260, 76–85. [PubMed: 24942683]

Heiss CN, and Olofsson LE (2018). Gut Microbiota-Dependent Modulation of Energy Metabolism. J Innate Immun 10, 163–171. [PubMed: 29131106]

Hotamisligil GS (2017). Inflammation, metaflammation and immunometabolic disorders. Nature 542, 177–185. [PubMed: 28179656]

Ko HJ, and Chang SY (2015). Regulation of intestinal immune system by dendritic cells. Immune Netw 15, 1–8. [PubMed: 25713503]

Koh A, De Vadder F, Kovatcheva-Datchary P, and Backhed F (2016). From Dietary Fiber to Host Physiology: Short-Chain Fatty Acids as Key Bacterial Metabolites. Cell 165, 1332–1345. [PubMed: 27259147]

Koppel N, Bisanz JE, Pandelia ME, Turnbaugh PJ, and Balskus EP (2018). Discovery and characterization of a prevalent human gut bacterial enzyme sufficient for the inactivation of a family of plant toxins. Elife 7.

Langmead B, and Salzberg SL (2012). Fast gapped-read alignment with Bowtie 2. Nature methods 9, 357–359. [PubMed: 22388286]

Lechner M, Findeiss S, Steiner L, Marz M, Stadler PF, and Prohaska SJ (2011). Proteinortho: detection of (co-)orthologs in large-scale analysis. BMC Bioinformatics 12, 124. [PubMed: 21526987]

Lee YS, Wollam J, and Olefsky JM (2018). An Integrated View of Immunometabolism. Cell 172, 22–40. [PubMed: 29328913]

Ley RE, Backhed F, Turnbaugh P, Lozupone CA, Knight RD, and Gordon JI (2005). Obesity alters gut microbial ecology. Proc Natl Acad Sci U S A 102, 11070–11075. [PubMed: 16033867]

Lumeng CN, Bodzin JL, and Saltiel AR (2007). Obesity induces a phenotypic switch in adipose tissue macrophage polarization. J Clin Invest 117, 175–184. [PubMed: 17200717]

Luo Y, Li W, Yu G, Yu J, Han L, Xue T, Sun Z, Chen S, Fang C, Zhao C, et al. (2017). Tsc1 expression by dendritic cells is required to preserve T-cell homeostasis and response. Cell Death Dis 8, e2553. [PubMed: 28079897]

Man K, Kutyavin VI, and Chawla A (2017). Tissue Immunometabolism: Development, Physiology, and Pathobiology. Cell Metab 25, 11–26. [PubMed: 27693378]

Maruvada P, Leone V, Kaplan LM, and Chang EB (2017). The Human Microbiome and Obesity: Moving beyond Associations. Cell Host Microbe 22, 589–599. [PubMed: 29120742]

Moor K, Fadlallah J, Toska A, Sterlin D, Balmer ML, Macpherson AJ, Gorochov G, Larsen M, and Slack E (2016). Analysis of bacterial-surface-specific antibodies in body fluids using bacterial flow cytometry. Nature protocols 11, 1531–1553. [PubMed: 27466712]

Morton GJ, Meek TH, and Schwartz MW (2014). Neurobiology of food intake in health and disease. Nat Rev Neurosci 15, 367–378. [PubMed: 24840801]

Nicholson JK, Holmes E, Kinross J, Burcelin R, Gibson G, Jia W, and Pettersson S (2012). Host-gut microbiota metabolic interactions. Science 336, 1262–1267. [PubMed: 22674330]

Patsouris D, Li PP, Thapar D, Chapman J, Olefsky JM, and Neels JG (2008). Ablation of CD11c-positive cells normalizes insulin sensitivity in obese insulin resistant animals. Cell Metab 8, 301–309. [PubMed: 18840360]

Peterson DA, McNulty NP, Guruge JL, and Gordon JI (2007). IgA response to symbiotic bacteria as a mediator of gut homeostasis. Cell Host Microbe 2, 328–339. [PubMed: 18005754]

Saxton RA, and Sabatini DM (2017). mTOR Signaling in Growth, Metabolism, and Disease. Cell 168, 960–976. [PubMed: 28283069]

Schroeder BO, and Backhed F (2016). Signals from the gut microbiota to distant organs in physiology and disease. Nat Med 22, 1079–1089. [PubMed: 27711063]

Seemann T (2014). Prokka: rapid prokaryotic genome annotation. Bioinformatics 30, 2068–2069. [PubMed: 24642063]

Segata N, Bornigen D, Morgan XC, and Huttenhower C (2013). PhyloPhlAn is a new method for improved phylogenetic and taxonomic placement of microbes. Nature communications 4, 2304.

Shi X, Xiao C, Wang Y, and Tang H (2013). Gallic Acid Intake Induces Alterations to Systems Metabolism in Rats. Journal of Proteome Research 12, 991–1006. [PubMed: 23231653]

Silverman JD, Washburne AD, Mukherjee S, and David LA (2017). A phylogenetic transform enhances analysis of compositional microbiota data. Elife 6.

Sonnenburg JL, and Backhed F (2016). Diet-microbiota interactions as moderators of human metabolism. Nature 535, 56–64. [PubMed: 27383980]

Stappenbeck TS, and Virgin HW (2016). Accounting for reciprocal host-microbiome interactions in experimental science. Nature 534, 191–199. [PubMed: 27279212]

Tian XY, Ganeshan K, Hong C, Nguyen KD, Qiu Y, Kim J, Tangirala RK, Tontonoz P, and Chawla A (2016). Thermoneutral Housing Accelerates Metabolic Inflammation to Potentiate Atherosclerosis but Not Insulin Resistance. Cell Metab 23, 165–178. [PubMed: 26549485]

Tian Y, Zhang LM, Wang YL, and Tang HR (2012). Age-Related Topographical Metabolic Signatures for the Rat Gastrointestinal Contents. Journal of Proteome Research 11, 1397–1411. [PubMed: 22129435]

Tremaroli V, and Backhed F (2012). Functional interactions between the gut microbiota and host metabolism. Nature 489, 242–249. [PubMed: 22972297]

Turnbaugh PJ, Hamady M, Yatsunenko T, Cantarel BL, Duncan A, Ley RE, Sogin ML, Jones WJ, Roe BA, Affourtit JP, et al. (2009). A core gut microbiome in obese and lean twins. Nature 457, 480–484. [PubMed: 19043404]

Turnbaugh PJ, Ley RE, Mahowald MA, Magrini V, Mardis ER, and Gordon JI (2006). An obesity-associated gut microbiome with increased capacity for energy harvest. Nature 444, 1027–1031. [PubMed: 17183312]

Valdearcos M, Douglass JD, Robblee MM, Dorfman MD, Stifler DR, Bennett ML, Gerritse I, Fasnacht R, Barres BA, Thaler JP, et al. (2017). Microglial Inflammatory Signaling Orchestrates the Hypothalamic Immune Response to Dietary Excess and Mediates Obesity Susceptibility. Cell Metab 26, 185–197 e183. [PubMed: 28683286]

Wang Q, Garrity GM, Tiedje JM, and Cole JR (2007). Naive Bayesian classifier for rapid assignment of rRNA sequences into the new bacterial taxonomy. Appl Environ Microbiol 73, 5261–5267. [PubMed: 17586664]

Wang Y, Huang G, Zeng H, Yang K, Lamb RF, and Chi H (2013). Tuberous sclerosis 1 (Tsc1)-dependent metabolic checkpoint controls development of dendritic cells. Proc Natl Acad Sci U S A 110, E4894–4903. [PubMed: 24282297]

Waterson MJ, and Horvath TL (2015). Neuronal Regulation of Energy Homeostasis: Beyond the Hypothalamus and Feeding. Cell Metab 22, 962–970. [PubMed: 26603190]

Yao L, Seaton SC, Ndousse-Fetter S, Adhikari AA, DiBenedetto N, Mina AI, Banks AS, Bry L, and Devlin AS (2018). A selective gut bacterial bile salt hydrolase alters host metabolism. Elife 7.

Zheng X, Qiu Y, Zhong W, Baxter S, Su M, Li Q, Xie G, Ore BM, Qiao S, Spencer MD, et al. (2013). A targeted metabolomic protocol for short-chain fatty acids and branched- chain amino acids. Metabolomics : Official journal of the Metabolomic Society 9, 818–827. [PubMed: 23997757]

Highlights

mTORC1 activation in $CD11c^{+}$ cells regulates food intake and body mass

Food intake and body mass are dependent on the microbiota of $Tsc1^{f/f}CD11c^{Cre}$ mice

Lactobacillus johnsonii Q1–7 is reduced in the microbiota of $Tsc1^{f/f}CD11c^{Cre}$ mice

L. johnsonii Q1–7 rescues food intake and body mass in $Tsc1^{f/f}CD11c^{Cre}$ mice

Context and Significance

Gut bacteria and inflammation have been linked to the development of obesity and type 2 diabetes. However, it is not known how the gut bacteria interact with the immune system to regulate body weight in healthy animals. We asked this question by activating the nutrient sensing pathway in a subset of immune cells. We found that activation of nutrient sensing in immune cells led to decreased weight gain in mice, which was dependent on their gut bacteria. Comparative analysis of the gut bacteria identified a specific strain of *Lactobacillus johnsonii,* which could rescue food intake and body weight in mutant mice. Our findings reveal the existence of transkingdom immune-bacteria circuits that regulate food intake and body mass in healthy animals.

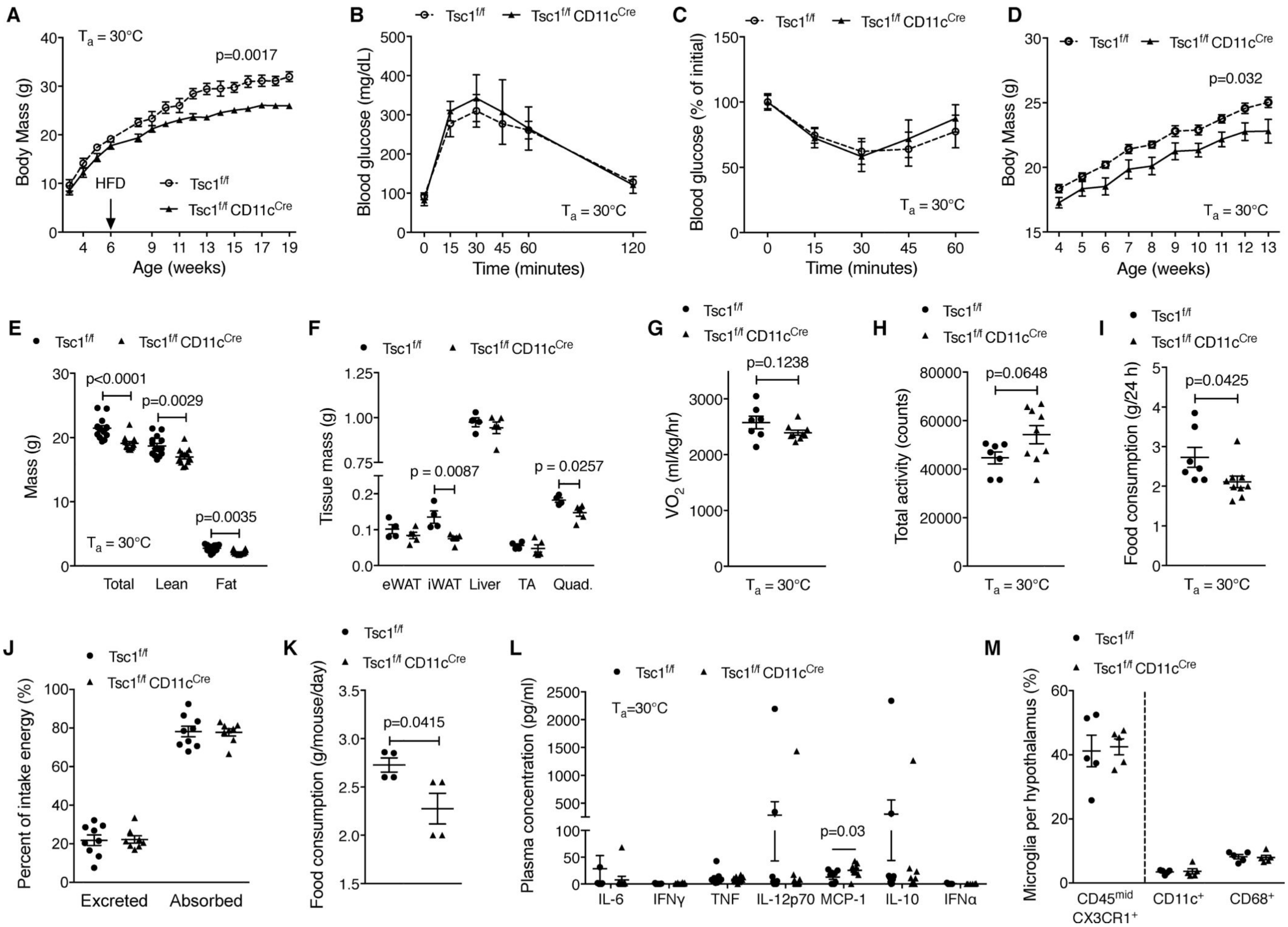

Figure 1. Activation of mTORC1 signaling in CD11c cells reduces body mass and food intake.

(A) Body mass of Tsc1$^{f/f}$ and Tsc1$^{f/f}$CD11c^{Cre} male mice fed high fat diet (HFD) from age of 6 to 19 weeks (n=6–8 per genotype; analyzed by two-way ANOVA). (B, C) Glucose (B) and insulin (C) tolerance tests of Tsc1$^{f/f}$ and Tsc1$^{f/f}$CD11c^{Cre} male mice fed HFD (n=4–5 per genotype; analyzed by two-way ANOVA). (D) Body mass of Tsc1$^{f/f}$ and Tsc1$^{f/f}$CD11c^{Cre} male mice fed low-fat regular chow diet (n=5 per genotype; analyzed by two-way ANOVA). (E) Body composition analysis by DEXA of Tsc1$^{f/f}$ and Tsc1$^{f/f}$CD11c^{Cre} male mice fed low-fat regular chow diet (n=14 per genotype; analyzed by t-test). (F) Tissue mass of Tsc1$^{f/f}$ and Tsc1$^{f/f}$CD11c^{Cre} male mice fed low-fat regular chow diet (n=4–5 per genotype). (G-I) Oxygen consumption (G), total activity (H), and food consumption (I) over 24 hours in 8-week-old Tsc1$^{f/f}$ and Tsc1$^{f/f}$CD11c^{Cre} male mice (n=7–9 per genotype; analyzed by t-test). (J) Assessment of energy harvest in 8-week-old Tsc1$^{f/f}$ and Tsc1$^{f/f}$CD11c^{Cre} male mice fed low-fat regular chow diet using fecal bomb calorimetry (n=8–9 per genotype; analyzed by t-test). (K) Food consumption in Tsc1$^{f/f}$ and Tsc1$^{f/f}$CD11c^{Cre} male mice after a 24 hour fast (n=4 per genotype). (L) Plasma concentrations of inflammatory cytokines in 8-week-old Tsc1$^{f/f}$ and Tsc1$^{f/f}$CD11c^{Cre} male mice fed low-fat regular chow diet (n=5–10 per genotype; analyzed by t-test). (M) Flow cytometric analysis of microglial populations in hypothalami of Tsc1$^{f/f}$ and Tsc1$^{f/f}$CD11c^{Cre}

male mice fed low-fat regular chow diet. Total microglia ($CD45^{mid}CX3CR1^{+}$); $CD11c^{+}$ microglia ($CD45^{mid}CX3CR1^{+}CD11c^{+}$) and activated microglia ($CD45^{mid}CX3CR1^{+}CD68^{+}$), (n= 5 per genotype; analyzed by t-test). Dashed line designates that $CD11c^{+}$ and activated microglia are subsets of total microglia. Data are presented as mean ± SEM.

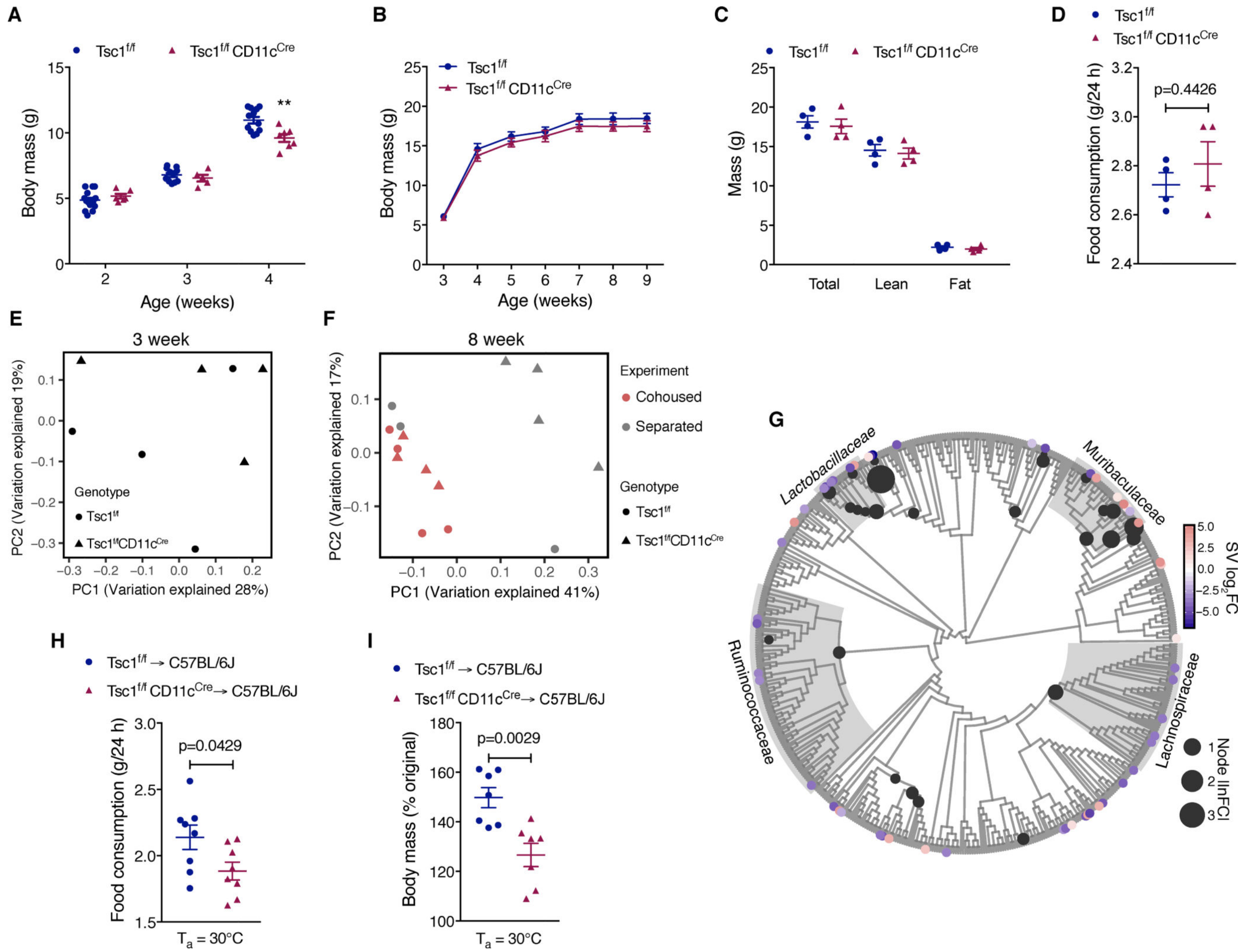

Figure 2. The gut microbiota of $Tsc1^{f/f}CD11c^{Cre}$ mice reduces food intake and body mass.

(A) Body mass of $Tsc1^{f/f}$ and $Tsc1^{f/f}CD11c^{Cre}$ mice on low-fat regular chow diet (n=5–15 per genotype; analyzed by t-test). (B-D) Body mass (B), body composition (C), and food consumption (D) in $Tsc1^{f/f}$ and $Tsc1^{f/f}CD11c^{Cre}$ mice fed low-fat regular chow diet and cohoused after weaning (n=4 per genotype; analyzed by two-way ANOVA (B) and t-test (C, D)). (E, F) PCoA using Bray Curtis dissimilarity for ordination of microbial communities of 3-week-old (E) or 8-week-old (F) $Tsc1^{f/f}$ and $Tsc1^{f/f}CD11c^{Cre}$ mice fed low-fat regular chow diet that were cohoused or housed separately. Each data point represents a single mouse at 3- (n=4 per genotype; analyzed by ADONIS p=0.368, R2=0.147 comparing genotypes) or 8-weeks of age (n=7–8 per genotype; analyzed by ADONIS p=0.002, R2=0.472 comparing separately-housed $Tsc1^{f/f}CD11c^{Cre}$ mice to separately-housed $Tsc1^{f/f}$ mice and cohoused mice). (G) Phylogenetic tree of 16S rRNA sequence variants and internal nodes that are significantly different between $Tsc1^{f/f}$ and $Tsc1^{f/f}CD11c^{Cre}$ mice housed separately. Black circles denote significantly different nodes analyzed by Welch's *t* test with multiple testing correction (FDR<0.1) with the size of the node representing absolute fold change. Colored tips denote significantly different sequence variants analyzed by DESeq2 (FDR<0.1) with color representing fold change comparing $Tsc1^{f/f}CD11c^{Cre}$ mice to $Tsc1^{f/f}$

mice. Bacterial clades of interest are highlighted in grey. (H, I) Change in body mass (H) and food consumption (I) in C57BL/6J mice after 8 weeks of oral gavage of fecal contents from $Tsc1^{f/f}CD11c^{Cre}$ or $Tsc1^{f/f}$ mice (n=7 per genotype; analyzed by t-test). Data are presented as mean ± SEM.

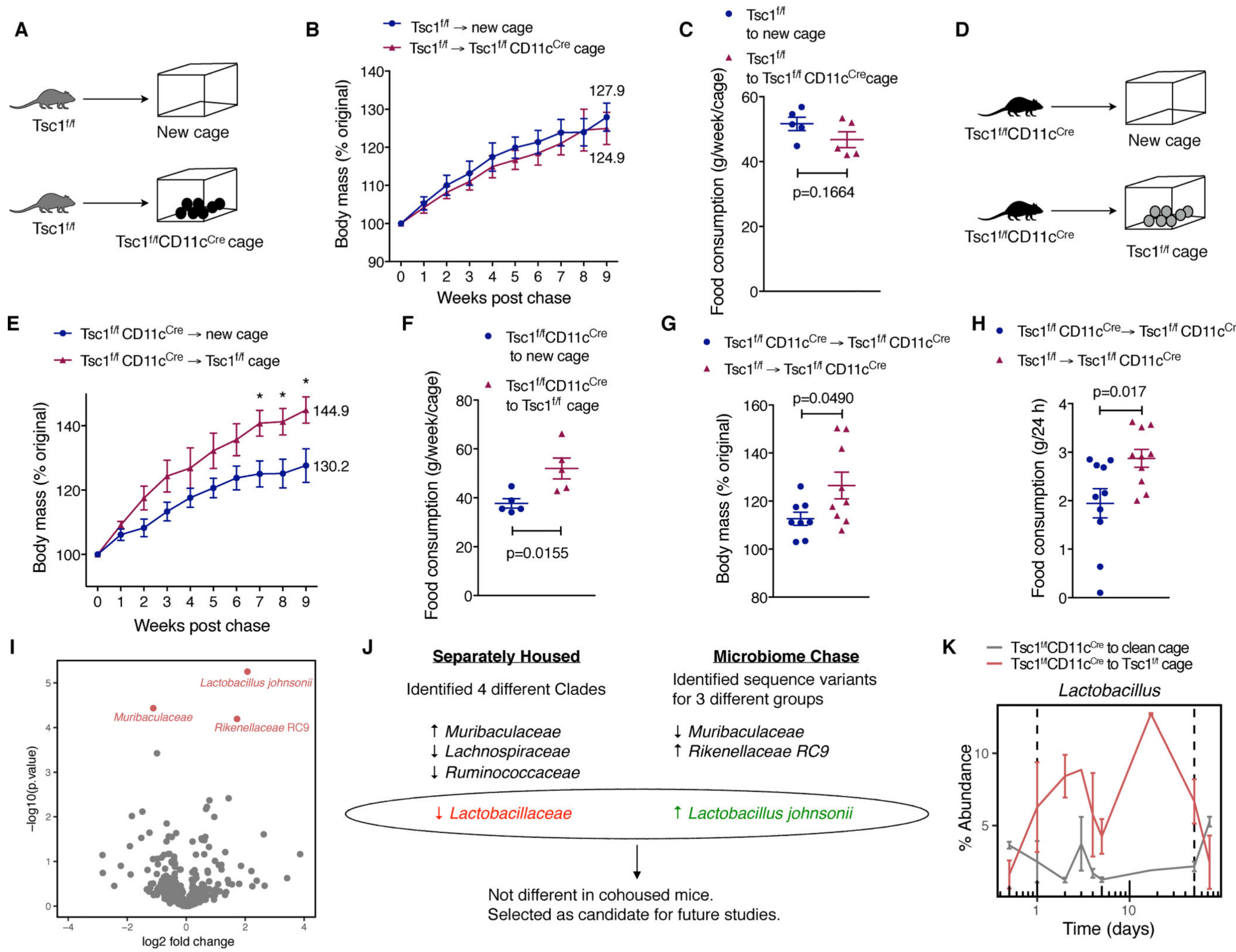

Figure 3. Abundance of *L. johnsonii* is reduced in microbiota of Tsc1$^{f/f}$CD11c^{Cre} mice.

(A) Schematic of Tsc1$^{f/f}$ mice being chased by the gut microbiota of Tsc1$^{f/f}$CD11c^{Cre} mice. (B, C) Change in body mass (B) and food intake (C) of Tsc1$^{f/f}$ mice during chase with the gut microbiota of Tsc1$^{f/f}$CD11c^{Cre} mice, (n=4–5, analyzed by 2-way ANOVA with Sidak's multiple comparisons test (B) and t-test (C)). (D) Schematic of Tsc1$^{f/f}$CD11c^{Cre} mice being chased by the gut microbiota of Tsc1$^{f/f}$ mice. (E, F) Change in body mass (E) and food consumption (F) in Tsc1$^{f/f}$CD11c^{Cre} mice during chase with the gut microbiota of Tsc1$^{f/f}$ mice, (n=4–5, analyzed by 2-way ANOVA with Sidak's multiple comparisons test (E) and t-test (F)). (G, H) Change in body mass (G) and food consumption (H) after 8 weeks of oral gavage of fecal contents from Tsc1$^{f/f}$CD11c^{Cre} or Tsc1$^{f/f}$ mice into Tsc1$^{f/f}$CD11c^{Cre} mice (n=8–9 per genotype; analyzed by t-test). (I) Volcano plot of 16S rRNA gene sequence variants that were different between Tsc1$^{f/f}$CD11c^{Cre} moved to clean cage or chased with the gut microbiota of Tsc1$^{f/f}$ mice. Red dots represent statistically significant sequence variants (analyzed by linear mixed effects model; log2 fold change>1 and FDR<0.1). (J) Schematic of the flowchart used to identify *L. johnsonii* as being less abundant in the gut microbiota of Tsc1$^{f/f}$CD11c^{Cre} mice. (K) Changes in relative abundance of *L. johnsonii* in stool of Tsc1$^{f/f}$CD11c^{Cre} mice during chase with the gut microbiota of Tsc1$^{f/f}$ mice (as in E, F). The dashed lines denote the period of microbiota chase experiment, (n = 2 per chase group; error bars represent range; analyzed by linear mixed effects model FDR<0.1). Data are presented as mean ± SEM.

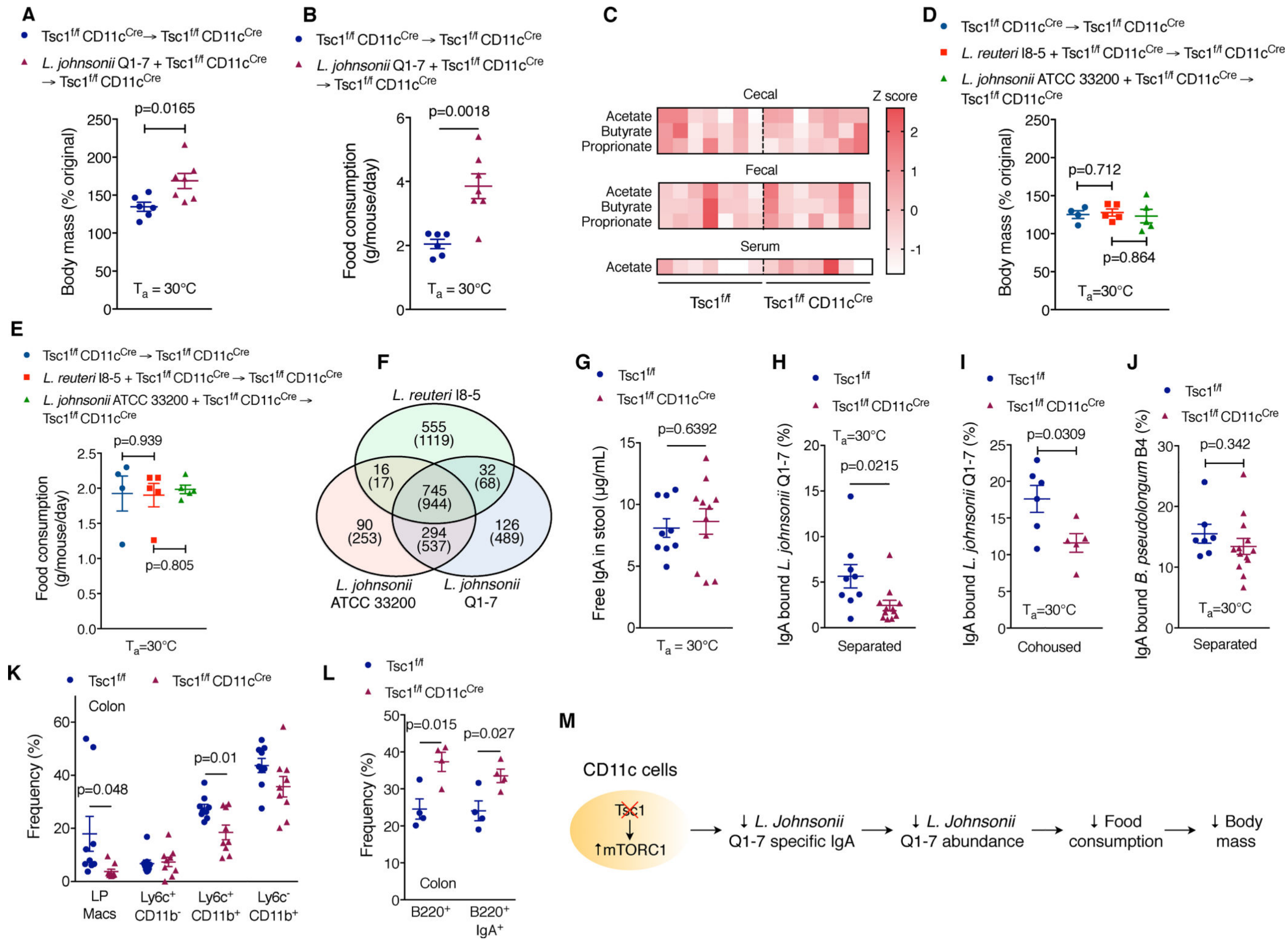

Figure 4. Reconstitution of *L. johnsonii* Q1–7 increases food intake and body mass in Tsc1$^{f/f}$CD11c^{Cre} mice.

(A, B) Change in body mass (A) and food intake (B) of Tsc1$^{f/f}$ CD11c^{Cre} mice orally gavaged with fecal contents of Tsc1$^{f/f}$ CD11c^{Cre} mice that were supplemented with vehicle or *L. johnsonii* Q1–7 (5×10^9 cfu) for 6 weeks, (n=6–7 per condition; analyzed by t-test). (C) Quantification of cecal, fecal, and plasma short chain fatty acids by GC-MS (n=7 per genotype; analyzed by Mann-Whitney). (D, E) Change in body mass (D) and food intake (F) of Tsc1$^{f/f}$ CD11c^{Cre} mice orally gavaged with fecal contents of Tsc1$^{f/f}$ CD11c^{Cre} mice that were supplemented with vehicle, *L. reuteri* I8–5, or *L. johnsonii* ATCC 33200 (5×10^9 cfu) for 6 weeks, (n=4–5 per condition; analyzed by t-test). (F) Shared gene content between lactobacilli genomes (number of annotated genes is indicated with hypotheticals included in parentheses). There are 126 annotated genes which are unique to the bioactive *L. johnsonii* Q1–7 genome (listed in Supplemental Table S2). (G) Quantification of free IgA in stool of 4-week-old Tsc1$^{f/f}$ and Tsc1$^{f/f}$CD11c^{Cre} mice (n=9–11 per genotype; analyzed by t-test). (H, I) Quantification of free IgA specific for *Lactobacillus* strain Q1–7 in stool of 4-week-old separated (H) or cohoused (I) Tsc1$^{f/f}$ and Tsc1$^{f/f}$CD11c^{Cre} mice (n=9–11 per genotype for separated and n=5–6 per genotype for cohoused; analyzed by t-test). (J) Quantification of free IgA specific for *B. pseudolongum* B4 in stool of 4-week-old separated Tsc1$^{f/f}$ and

$Tsc1^{f/f}CD11c^{Cre}$ mice (n=7–13 per genotype for separated; analyzed by t-test). (K, L) Quantification by flow cytometry of $CD11c^{+}$ macrophages (K, n=9 per genotype) and B cells (L, n=4 per genotype) in lamina propria of colons of 8-week-old $Tsc1^{f/f}$ and $Tsc1^{f/f}CD11c^{Cre}$ mice (analyzed by t-test). (M) A working model for the transkingdom immune-microbiome interactions described here. Data are presented as mean ± SEM.